Raman Spectroscopy of pure and (Nb+In) co-doped TiO_2 single crystals

Nikiben Patel

Material Physics

Submitted in partial fulfillment of
the requirements for the degree of

Master of Science

Faculty of Science and Mathematics, Brock University
St. Catharines, Ontario.

Abstract

This research project focused on the study of pure TiO_2 rutile crystals and rutile crystals that were 2% co doped with Niobium and Indium TiO_2 (2-NITO). There has been a growing interest in co-doped TiO_2 due to recent papers [6] [9]published on its "colossal permittivity" in the lower frequency range of 10^2 to 10^6 Hz. The goal of this study was to analyze the impact of co-doping on the Raman modes by using Raman spectroscopy. To determine the Raman shift and Half width at half max from the raman data, the Lorentz fit analysis was applied.

Acknowledgment

- Dr. David Crandles
- Dr. Maureen Reedyk
- Dr. Hiroki Taniguchi
- Jeremy Dion
- Collin Tower
- Connor Wilson

Table of Contents

List of Figures

Chapter 1

Introduction

1.1 Dielectric Permittivity

Electrons cannot freely travel through non-conductors (also known as dielectrics). As a result, when exposed to an external electric field $\overrightarrow{E}$, bulk dielectric materials form an internal displacement field $\overrightarrow{D}$. For a linear, isotropic, homogeneous dielectric permittivity(ϵ) is the ratio of the electric displacement(D) and the electric field(ϵ_o $\overrightarrow{E}$):

$$\overrightarrow{D} = \epsilon_o \tilde{\epsilon} \overrightarrow{E} \tag{1.1}$$

where $\tilde{\epsilon} = \epsilon_1 + i\epsilon_2$ is the permittivity

The electric field, electric displacement and electric polarization are related by the following expression:

$$\overrightarrow{D} = \epsilon_o \overrightarrow{E} + \overrightarrow{P} \tag{1.2}$$

where ϵ_o is the permittivity of free-space defines the relationship between $\overrightarrow{D}$ and $\overrightarrow{E}$ if the material is non-polarizable (when $\epsilon = 1$) . Therefore, the dielectric permittivity and the electric displacement define how strongly a material becomes electrically polarized under the influence of an electric field.

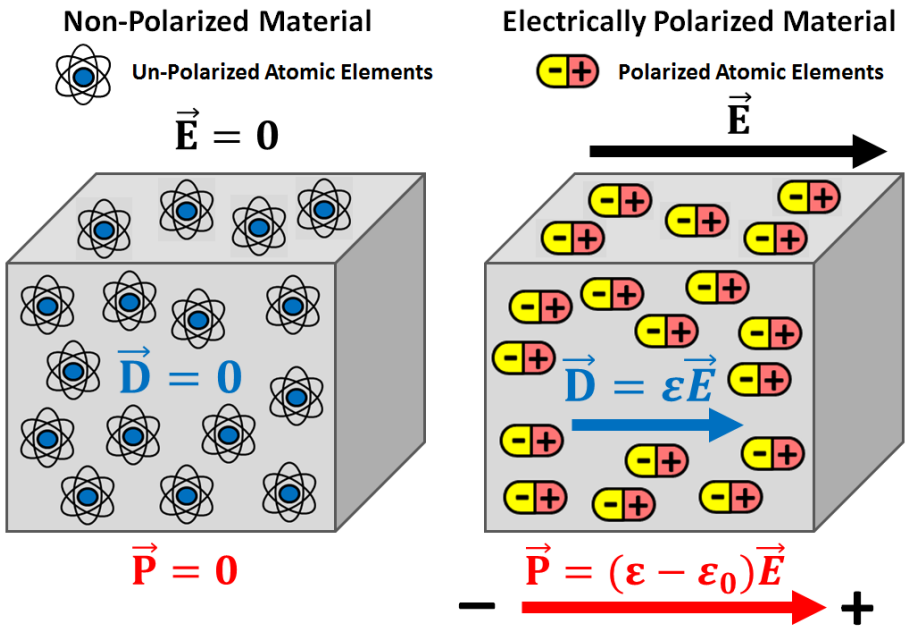

Figure 1.1: Polarization of Dielectric materials.[5]

The relative permittivity (or dielectric function) ϵ_r of a dielectric is the ratio of permittivity ϵ to free space permittivity ϵ_0. The permittivity is the real part of a dielectric function. Dielectric permittivity is an interesting phenomenon with numerous practical applications.

1.2 Colossal Permittivity(CP)

In most common materials ϵ is a complex value with its real part usually less than a value of 100 in the lower frequency ranges (0.1 MHz). If a material has a permittivity of about 1000 or greater, it is considered to exhibit colossal permittivity (CP). For some common materials, such as water, $\epsilon \approx 80$, while many industrial materials have $\epsilon < 100$.

Large permittivitiy materials are of great interest due to their possible applications in energy storage devices. The energy stored per unit volume of a dielectric material (J), is:

$$J = \int_0^{D_{max}} \vec{E}.d\vec{D} \tag{1.3}$$

where E is the electric field and D_{max} is the electric displacement(D) at the highest field applied.

1.2.1 Research on CP

Recent research and development have been greatly influenced by the incredible potential of colossal permittivity (CP) materials for use in modern microelectronics as well as for high-energy-density storage applications. Modern electrical systems require high energy-density storage devices, such as those found in cordless power tools and hybrid electric vehicles, which super-capacitors can fill. Since liquid dielectric material is currently used in super-capacitors, solid CP materials may improve super-capacitors by enhancing their energy density and safety. It is not essential to create a pure compound for CP. These CP materials have undergone extensive research. Doping a parent material is a well-known method for producing high-permittivity materials.

CP was discovered in $CaCu_3Ti_4O_{12}$. Many CP compounds have been discovered since then that exhibit the $CaCu_3Ti_4O_{12}$ perovskite-like crystal structure such as $Bi_{2/3}Cu_3Ti_4O_{12}$ and rare-earth element-based materials $Ln_{2/3}Cu_3Ti_4O_{12}$ where Ln = La, Ce, Pr, Nd, Sm, Eu, Gd, Tb, Dy, Ho, Er, Tm (a trivalent rare earth element) (CCTO) around the year 2000. Despite the development of many new classes of CP materials, the discovery of such materials with the required high performance is still a highly challenging task. Hu et.al. [6] proposed a new electron-pinned, defect-dipole mechanism to ideal CP behaviour, where hopping electrons are localized by designated lattice defect states to generate giant defect-dipoles and result in high-performance CP materials [6]. In 2013, Hu et al. reported in their work that TiO_2 co-doped with different percentages of In and Nb showed CP which, importantly, shows low dielectric loss (ϵ_2) that is mostly temperature and frequency independent.

1.3 Rutile-TiO_2

TiO_2 is promising material, so many researchers study it for various applications like sensors, purification and disinfection of wastewater, self-cleaning coatings for buildings, photovoltaics and photocatalysis.

Rutile is an intriguing material because it has one of the highest ϵ_1 values, which increases as temperature decreases. It is the most common naturally occurring form. Due to its abundance, low toxicity, and largest permittivity among binary oxides (around 260 along the c-axis), rutile makes an excellent host for doping.

Titanium dioxide exists in three main polymorphic structures: Rutile is the most common naturally occurring form of TiO_2, the others being Anatase and Brookite. Rutile has two TiO_2 molecules in the unit cell with space group $D_{4h}^{14}(P4_2/mnm)$. Rutile has a remarkable amount of refraction and birefringence and is uniaxial.

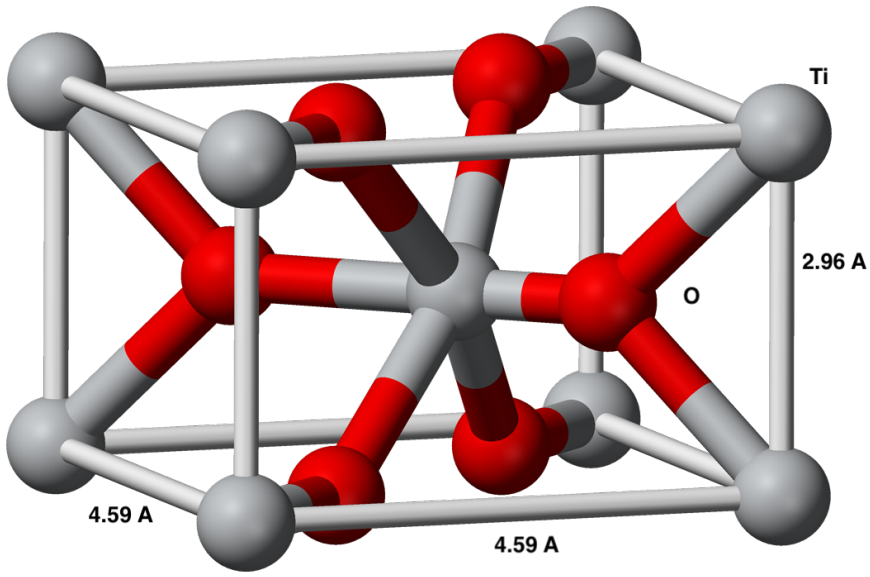

Figure 1.2: Crystal Structure of Rutile TiO_2. [3]

Rutile crystals are most commonly observed to exhibit a prismatic growth habit with orientation along their c axis. The growth habit of rutile is favored as the (110) facets exhibits the lowest surface free energy therefore they are thermodynamically most stable. The c-axis oriented growth of rutile appears clearly in nanorods and nanowires.

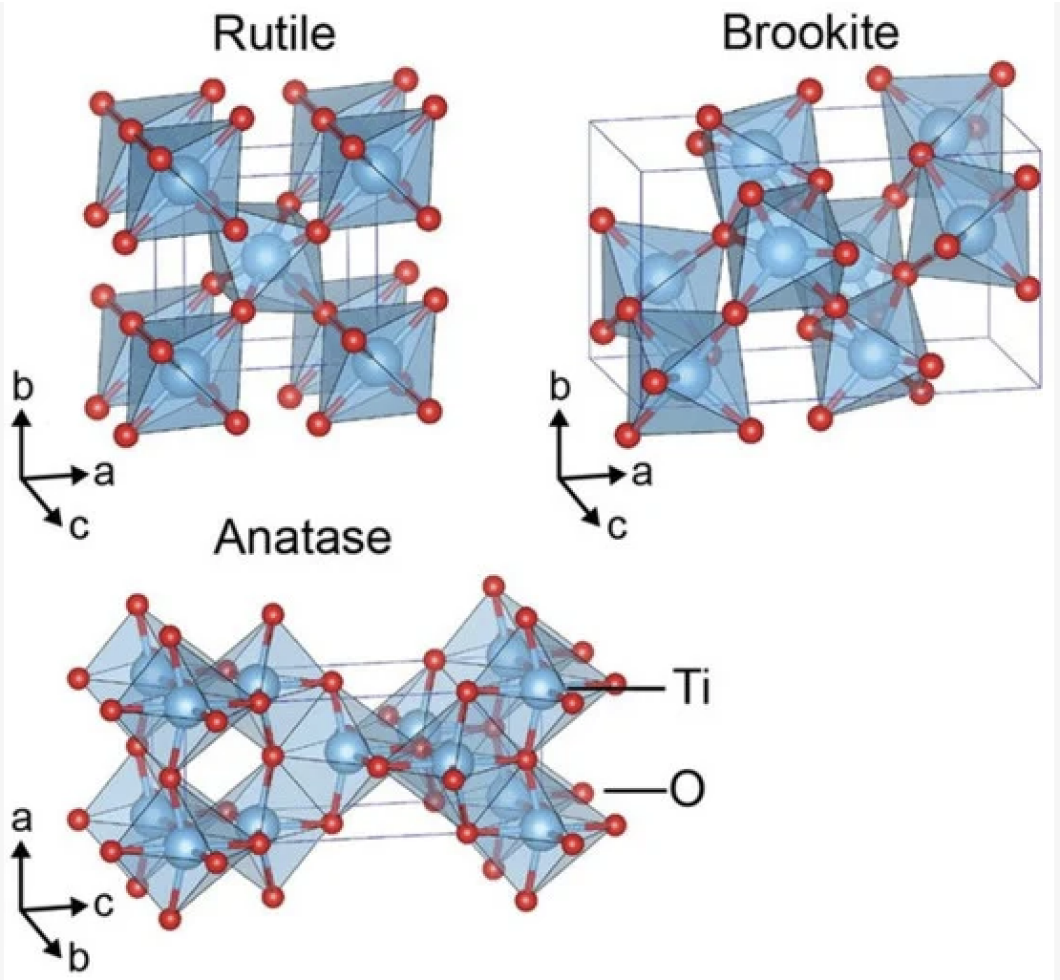

Figure 1.3: Different Structures of TiO_2. [2].

There are phonon dispersion branches in a 3-D structure. (3p-3) are optical branches,where p is the number of atoms per unit cell. That contributes to total 15 vibrational modes [1]. A group theory analysis of rutile TiO_2 done by P.S.Narayanan shows that these 15 modes have following representations : $1A_{1g} + 1A_{2g} + 1A_{2u} + 1B_{1g} + 1B_{2g} + 2B_{1u} + 1E_g + 3E_u$ where symbol g represents Raman active, u infrared active and E is 2-fold degenerate modes. Further revelations showed that four modes A_{1g},B_{1g}, B_{2g}, E_g are Raman active modes. Four modes A_{2u} and $3E_u$ are IR active. Three modes A_{2g} and $2B_{1u}$ are neither Raman active nor IR active [8]. The E_u modes here are active with the electric field perpendicular to the c-axis, and the A_{2u} mode is active with the electric field parallel to the c-axis. [9]

1.4 Electron Pinned Defect Dipole (EPDD)

Electron pinned defect dipoles (EPDD) are a potential alternative method for engineering large ϵ_1, which was first studied in TiO_2. An electron pinned defect dipole (EPDD) is created by heteroatomically substituting atoms into a parent metal oxide. The best-known example is doping TiO_2 with equal parts of both donor and acceptor. According to the EPDD model, the acceptor causes localised oxygen deficiency, which pins electrons from the donor. This results in a forming of a defect-dipole complex made of a local combination of a partially delocalized electron, substituted hetero-atoms (i.e. the donor and acceptor atoms) and reduced host cations.[6]

Hu et al. [6] demonstrated that co-doping rutile TiO_2 with equal parts Nb (a donor) and In (an acceptor) increased permittivity below 1MHz. The NITO notation is defined by the example: 2%(Nb+In)co doped TiO_2 = 2 - NITO. Co-doping with equal concentrations is critical of donors and acceptors because the Nb helps to create mobile electrons and the In helps to localise those electrons.

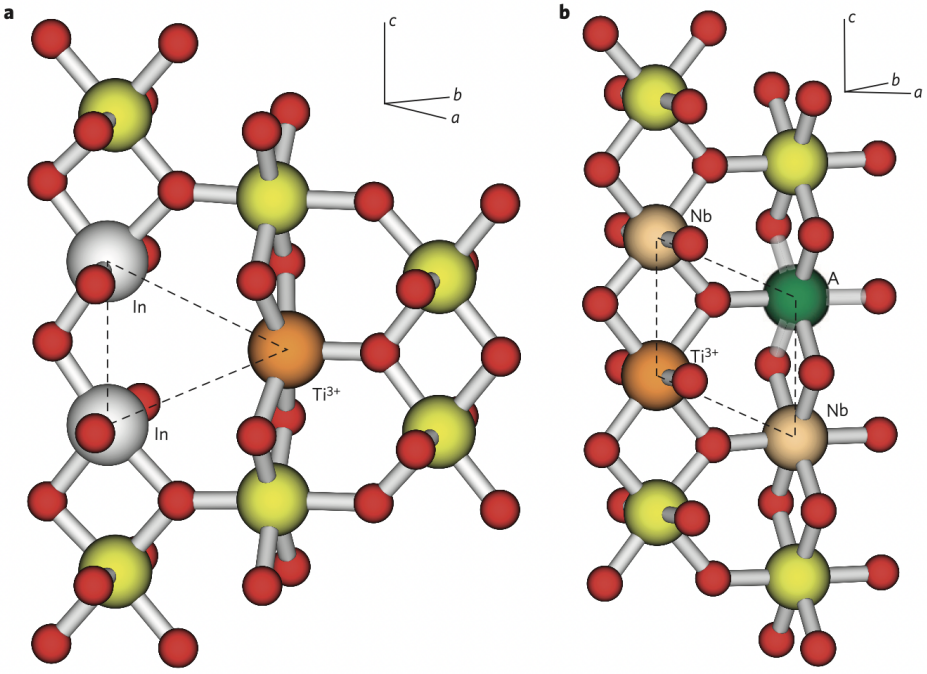

Figure 1.4: Structure of the In and Nb defect complexes. In diamond structure, A atom could be Ti^{+3} or In^{+3}.[6]

Furthermore, this material demonstrated low dielectric loss over a wide temperature range of 80 to 450 K, as well as over a wide frequency range. For example, 0.05% Nb+In co-doping

results in a room-temperature permittivity of 2×10^4, a dielectric loss of less than 0.05, and a frequency range of 10^1 to 10^5 Hz which offers the possibility of replacing the state-of-the-art CP materials.

Two structural motifs that are described in Fig. 1.4 are 'triangular' complex and a 'diamond'. The electrons in this system have more space to move around than atomic electrons, which results in large defect-dipoles that act more like dipoles caused by defects in the lattice structure rather than electrons moving around freely. The liberated electrons are locally bound by the oxygen deficient area and cannot hop through the structure, resulting in less dielectric loss than in purely donor doped TiO_2.

For example, TiO_2 is a simple metal oxide that may be representative of a large group of metal oxides able to produce high CP behaviour. Changing the dopants is another option. Preliminary research indicates that co-doping with Al^{+3} rather than In^{+3} causes CP behaviour.

1.5 Raman Spectroscopy

The Raman Effect is the inelastic scattering of light by lattice vibrations. Infrared active modes have odd Ungerade(u) symmetry, in which the dipole moment of the molecule changes with vibrations. Raman active modes have even Gerade(g) symmetry, in which the polarizability varies with vibration. To study these modes, a material is irradiated with photons of known energy. This is generally done with a high intensity laser.

1.5.1 Raman Scattering

A very small amount of photons either gain or lose energy during their scattering, occurring when the photon interacts with the vibrational state of a molecule. When a scattered photon loses energy, it is considered to be red-shifted. This is called Stokes scattering, and some of the photon's energy is transferred into vibrational energy of the molecule it scatters with,causing the molecule to reach an excited state. The opposite of this is known as anti-Stokes scattering, which occurs when the incident light interacts with a molecule in an excited state. This leaves the photon blue-shifted, and does not often occur at room temperature because very few molecules reside in the excited state. In both Stokes and anti-Stokes scattering, the energy lost or gained through the interaction is equal to the energy required for an excited state transition to occur.

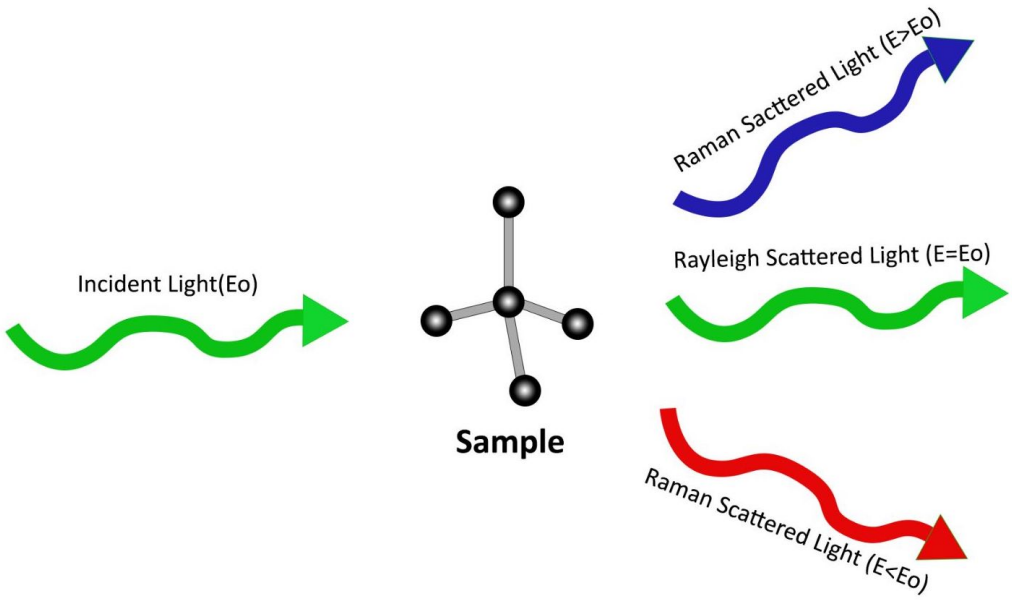

Figure 1.5: Schematic of Raman Scattering

1.5.2 Rayleigh scattering

When a photon interacts with an atom it usually experiences Rayleigh elastic scattering. In this type of interaction, the scattered photon has the same energy as the incident photon. This type of scattering occurs nearly 100% of the time during a measurement

1.5.3 Raman Spectroscopy vs Infrared Spectroscopy

Both techniques involve measuring light that has interacted with a material, but they are distinct from each other. By using both methods on a sample, it is possible to gain a deeper understanding of the dynamics of the material's lattice structure. The differences between these techniques is:

- Raman spectra are generated by the scattering of light by vibrating molecules, while IR spectra are produced by the absorption and re-emission of light by vibrating molecules.
- Raman activity is caused by a change in the polarizability of a molecule, while IR activity is caused by a change in the dipole moment of a molecule.
- Raman measurements are typically done using a high-power, monochromatic laser that is in the visible spectrum while IR measurements are done using a low-intensity, multi-color

light source such as a globar.

- Raman scattered light is typically measured at a 90-degree angle to the incident light beam, while IR re-emitted light is measured in the opposite direction as the initial beam to reduce the Rayleigh intensity in the case of normal incidence reflection.

1.6 Project Plan

The main focus of this project is to investigate Raman active modes of 2-NITO. In addition, pure titanium dioxide single crystals will also be measured for comparison. It is desirable to determine if there are new peaks in co-doped TiO_2 and to find out the effects of co-doping on peak width to determine the effects of co-doping on these modes.

Chapter 2

Materials and Methods

2.1 Sample Acquisition

Single crystals of 2-NITO samples in this study are obtained from the lab of Hiroki Taniguchi which was created using the Optical Floating zone crystal growth method.

2.2 Optical Floating zone crystal growth

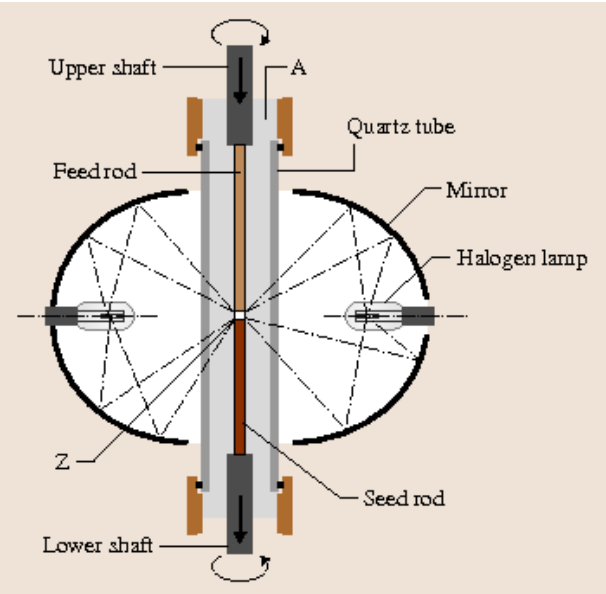

Figure 2.1: Schematic diagram of optical floating zone apparatus.[4]

In Fig. 2.1, A – atmosphere, Z – floating zone. Two ceramic rods are positioned so that their ends meet at the focal point of ellipsoidal mirrors. The mirrors have lamps, either halogen or xenon, of the appropriate power level at their other focal points. The process of growing crystals begins by heating the ends of the polycrystalline rods to melt them and creating a liquid, called the floating zone, between the seed rod and the feed rod. The floating zone is moved upward, either by moving the mirrors or by moving the seed-and-feed setup downward, as the liquid cools and the material solidifies and forms crystals on the seed rod. [4]

2.3 Experimental Procedure

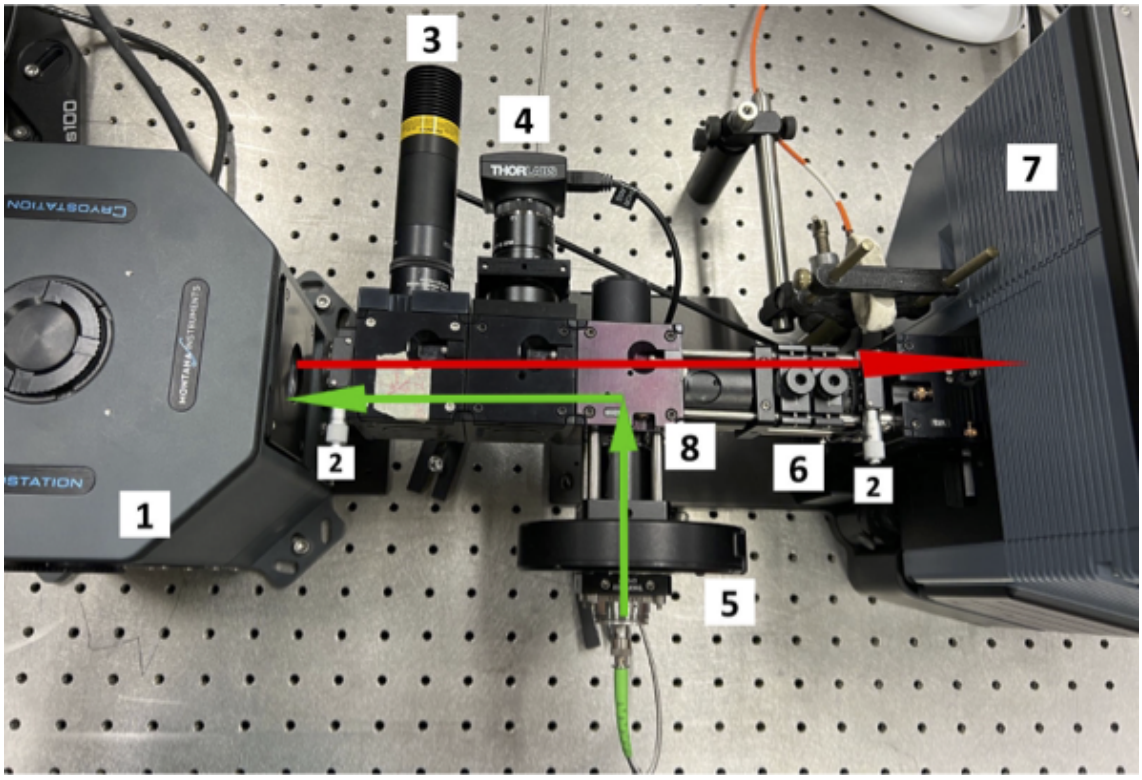

Figure 2.2: Back-scattering geometry setup of Raman Spectroscopy.

In Fig. 2.2 the green arrow shows the incident light path and the red arrow shoes the reflected polarisation. Raman measurements were performed using a Montana Instruments CryoRaman system, which includes a Cryostation s100-CO and a 100x 0.75NA objective, in conjunction with a Princeton Instruments FERGIE spectrometer. The setup uses a back scattering geometry. All samples were mounted using thermally conductive Apiezon N grease as instructed by the

manual for the machine. Measurements were taken at room temperature and at 4 K for which samples were cooled overnight. Measurements were taken after the samples had reached thermal equilibrium with a stability of 10mK. All the measurements were done at 1 mW without intensity reduction filter.

The Raman system was calibrated using 2-point calibration system which fixes two wavelength. Fixed Calibration relies on positions of known peaks of a known source such as a mercury or neon lamp.

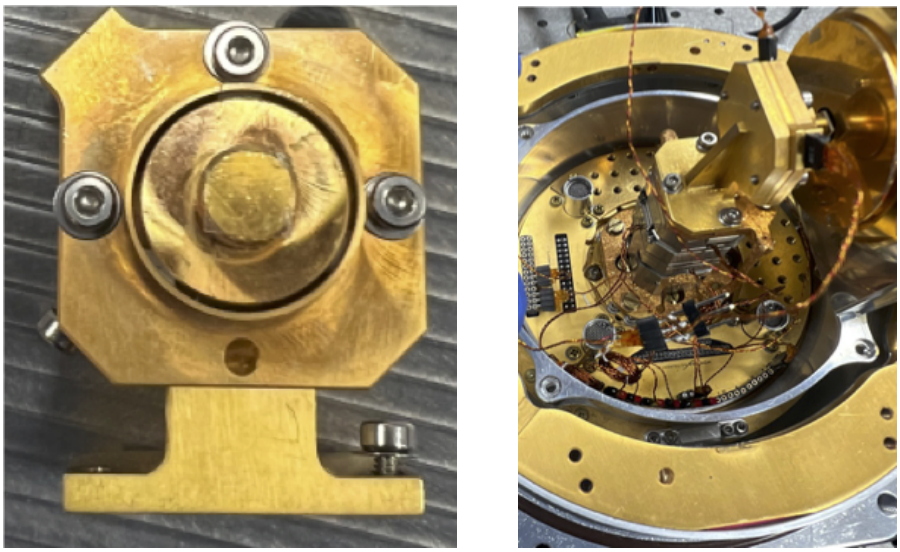

Figure 2.3: Sample Mount and Instrument interior

2.3.1 Porto Notation

It is important to keep track of the polarization conditions when making measurements in order to ensure consistent results. The Porto notation is a system for recording the orientation of a sample, the direction of the outgoing light, the orientation of the analyzer, and the polarization of the incident light. This notation includes four components :

a(bc)d

a is the excitation (laser) propagation direction,

b is the excitation (laser) polarisation direction,

c is the scattering (Raman) polarisation direction,

d is the scattering (Raman) propagation direction.

Chapter 3

Results and Discussion

3.1 TiO_2

The first Raman spectrum of rutile was recorded by P.Narayanan [8] and peak identifications were done by Porto[9]. Raman spectrometry has been utilized in various studies investigating the lattice movement, phase transition, and nanostructures of TiO_2.

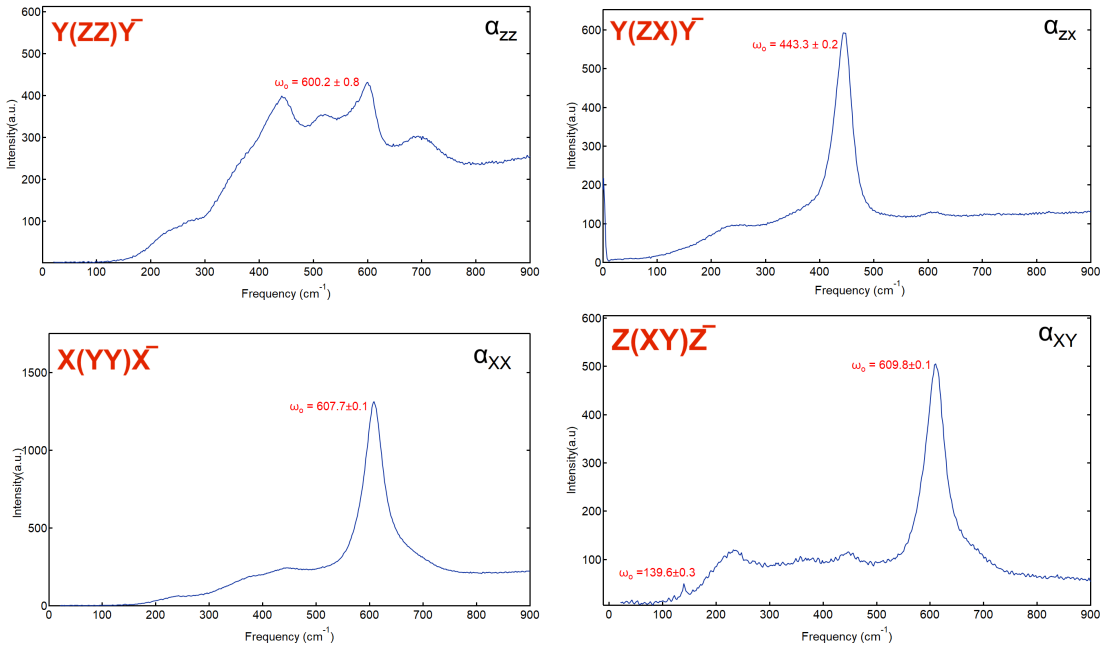

Figure 3.1: Raman Modes of TiO_2

Comparing our data with Porto there is fair agreement with their data with frequency shifts difference by 4cm^{-1} as seen in 3.1. The B_{1g} mode is observed in XY polarisation wheres in Porto paper it is in XX polarisation. This maybe due to the fact that here we are using back-scattering geometry setup whereas Porto used 90^o setup. The variation in the intensity of E_g and A_{1g} can be attributed to the difference in the measurement angles of the two samples relative to the polarized incident radiation. However, also seen in 3.1 is an additional mode not expected from group theory. This mode is around 235 cm^1 at T=300K for both crystals, and has a very large dependence on temperature. Porto, in his paper[9], observes that the peak mentioned is not a fundamental process since there is no simple symmetry with any one-phonon Raman tensors, and therefore it is a combination line. 3.1 details all the observed modes from both the a and c axes. The B_{2g} at 826cm^{-1} mode was seen by Porto in YX polarisation but we don't observe it in our data. It is too weak for obtaining quantitative information and is even difficult to resolve at low temperature with polarized Raman scattering.

3.2 2-NITO

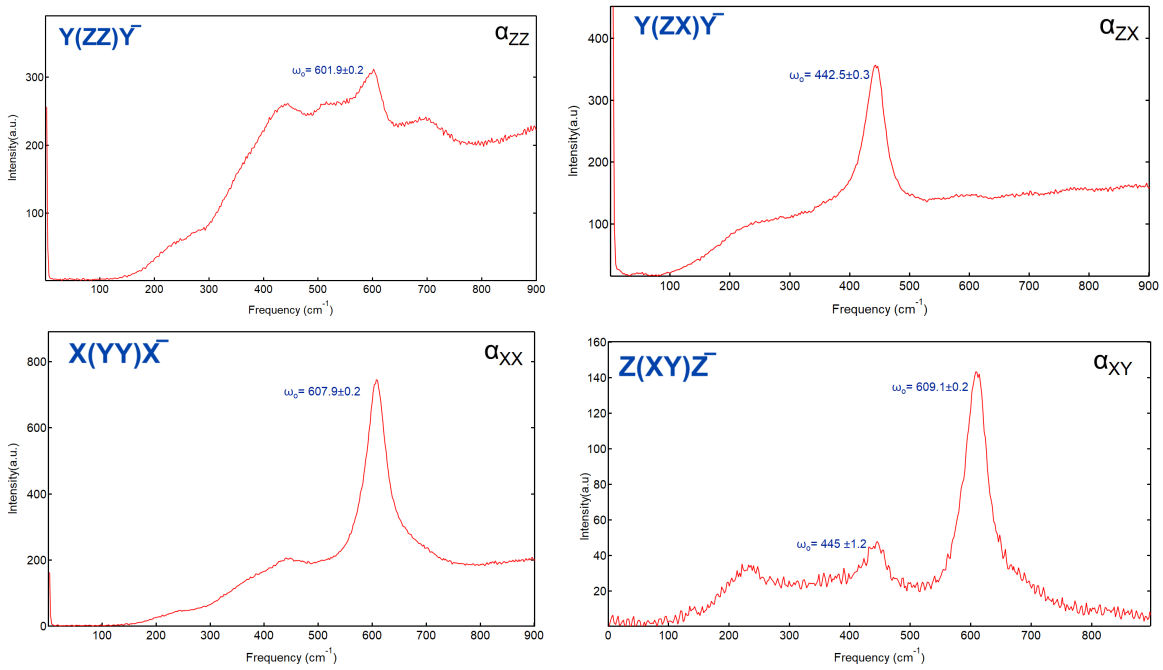

Figure 3.2: Raman Modes of NITO

Comparing 2-NITO data with TiO_2 all the modes were observed at same frequency but there is decrease in intensity. The B_{2g} at 826cm^{-1} mode was not seen in 2-NITO data too.

3.3 Comparison of TiO_2 and 2-NITO

Modes(cm^{-1})	TiO_2 Porto [9]	TiO_2 Lan [7]	TiO_2 This work	2-NITO(This Work)
B_{1g}	143	143	139.6 ± 0.3	143.5 ± 0.1
E_g	447	447	443 ± 0.2	442.5 ±0.3
A_{1g}	612	612	607.7 ±0.1	607.9 ±0.2

Table 3.1: Raman Modes observed from Spectra

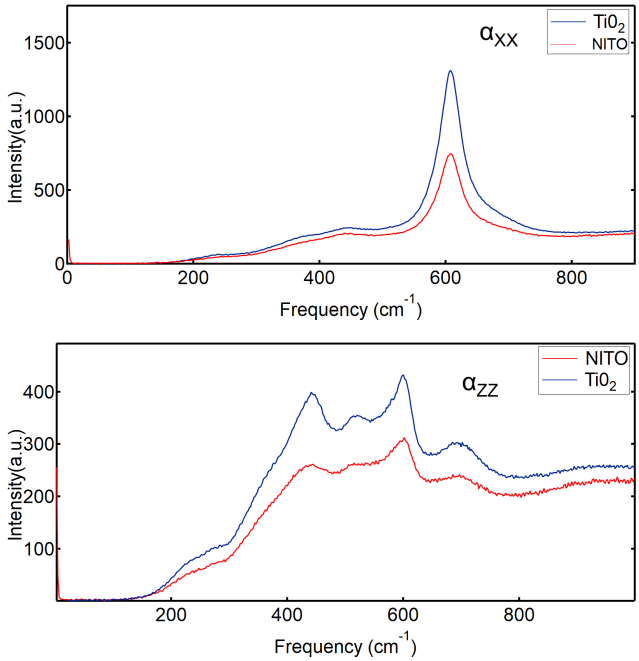

Figure 3.3: Different Polarisation of TiO_2 and 2-NITO

As seen in Fig. 3.6 the polarisation of both samples almost looks similar the intensity is low.

3.4 Lorentzian Fit

The function used for fitting is in the form:

$$I(\omega) = BG(\omega) + \sum_i \frac{A_i}{(\omega - \omega_{oi})^2 + \Gamma_i^2} \tag{3.1}$$

where BG(ω) is a linear background, A_i is the intensity of a peak, Γ_i is the Half Width Half Max(HWHM) of a peak and ω_{oi} is the peak position.

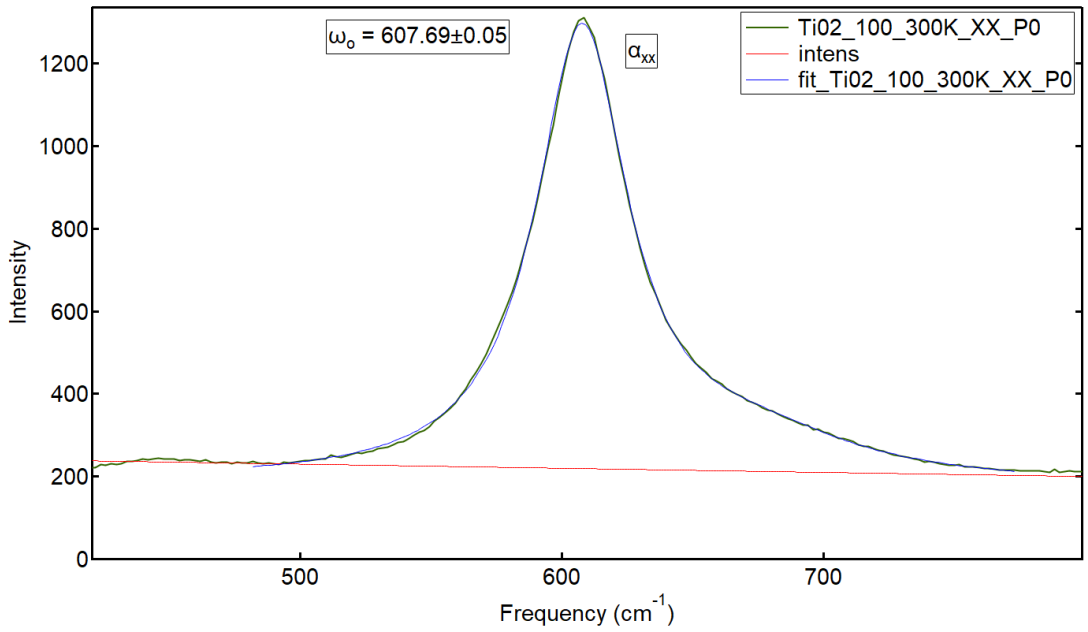

Figure 3.4: Lorentz fit done on wave

These Lorentzian fits were done on the two strongest modes (Eg and A1g) and compared to Lan's [7] parameters. Note there is a sizable shift between Lan's and ours peak positions seen in Figure , this discrepancy was also seen in Table 3.1. The most likely explanation for this difference is that the resolution of our instrument is rather poor, approximately 4.4cm^{-1} point spacing. The overall T-dependence is similar and our FWHM parameters are fairly close to literature, but again, the poor resolution could explain the deviation. When comparing 2-NITO's parameters to TiO_2's, we observe a small decrease in peak position in 2-NITO, as well as a small increase in FWHM, especially in the higher temperatures of the Eg mode. Besides the sizeable FWHM change, the overall effect due to doping appears to be minimal.

3.5 Frequency Shift and Peak Width

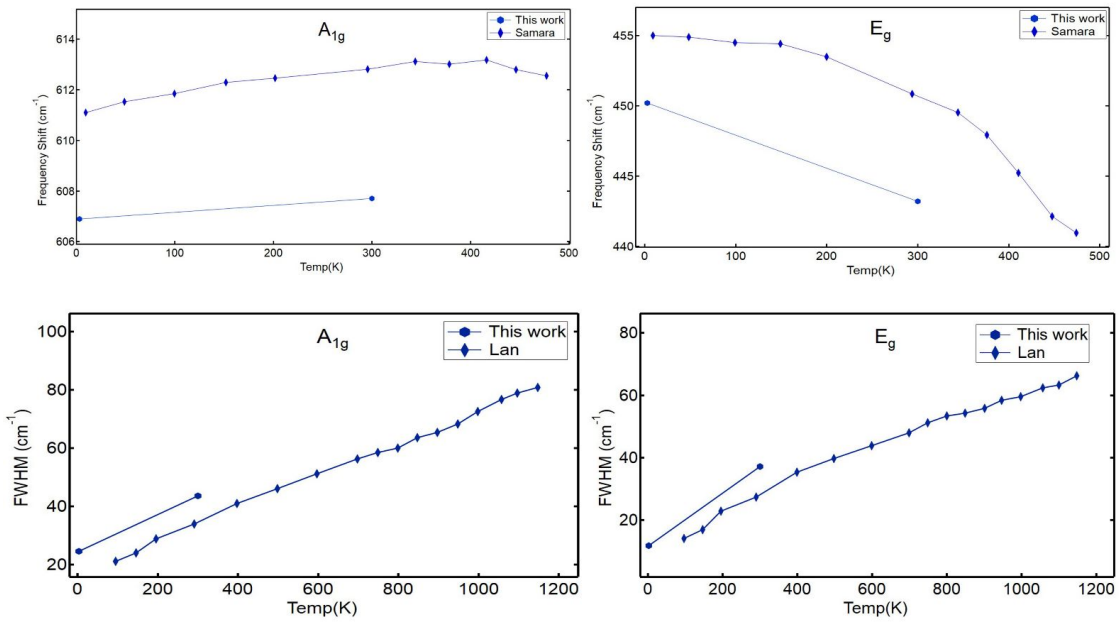

Figure 3.5: Data taken from Lan and Samara

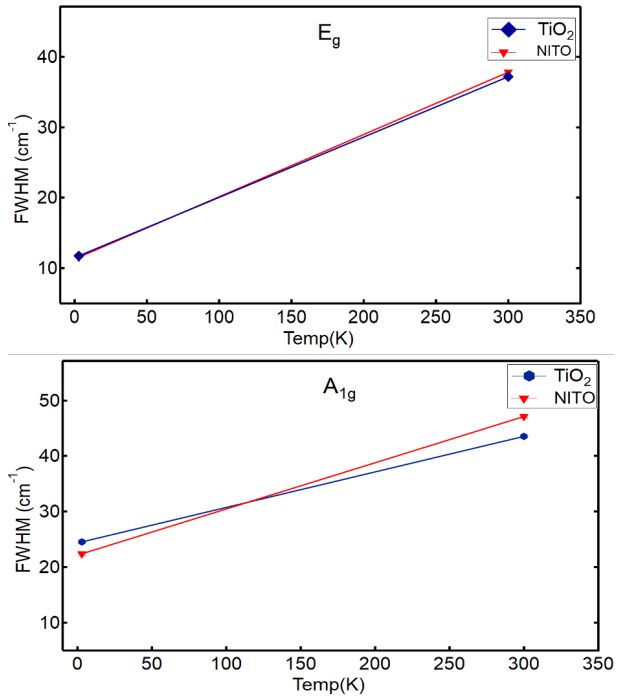

Figure 3.6: Parameters taken from Lorentzian fits of each mode

In Fig. 3.5, data is taken from T.Lan [7] and Samara [10] and was plotted against our data for comparison. As can be seen in fig., the trend is similar to what they published in their paper. The intensity of our data is less. Here, we have plotted data for just two temperatures whereas they have data over a range of temperatures.

The scattering intensity of the B_{2g}, phonon is relatively weak, and its temperature and intensity shifts so small that they could not be measured accurately

In a paper by Lan et al. [7], the author used the relationship between pressure and temperature and the shifts in Raman peaks to distinguish between harmonic and quasiharmonic behaviors. He discovered that the B_{1g} mode had a large quartic anharmonicity and a small cubic anharmonicity, while the E_g and A_{1g} modes were mainly dominated by cubic anharmonicity. Lan concluded that the anharmonic effects were mainly due to energy and momentum conservation during phonon-phonon scattering processes. With regards to ferroelectricty, Lan found no evidence of orthorhombic distortion, suggesting that the anharmonicity was caused by the phonon response to temperature and pressure, rather than an incipient phase transition [7].

Bibliography

[1] U. Balachandran and N.G. Eror. "Raman spectra of Titanium dioxide". In: *Journal of Solid State Chemistry* 42.3 (1982), pp. 276–282. ISSN: 0022-4596. DOI: https://doi.org/10.1016/0022-4596(82)90006-8. URL: https://www.sciencedirect.com/science/article/pii/0022459682900068.

[2] Metka Benčina et al. "Crystallized TiO_2 Nanosurfaces in Biomedical Applications". In: *Nanomaterials* 10.6 (2020). ISSN: 2079-4991. DOI: 10.3390/nano10061121. URL: https://www.mdpi.com/2079-4991/10/6/1121.

[3] "Benjah-bmm27, Public domain, via Wikimedia Commons". In: (30 April 2007). URL: https://en.wikipedia.org/wiki/Titanium_dioxide#/media/File:Rutile-unit-cell-3D-balls.png.

[4] Hanna A. Dabkowska and Antoni B. Dabkowski. "Crystal Growth of Oxides by Optical Floating Zone Technique". In: *Springer Handbook of Crystal Growth*. Ed. by Govindhan Dhanaraj et al. Berlin, Heidelberg: Springer Berlin Heidelberg, 2010, pp. 367–391. ISBN: 978-3-540-74761-1. DOI: 10.1007/978-3-540-74761-1_12. URL: https://doi.org/10.1007/978-3-540-74761-1_12.

[5] "Dielectric Permittivity". In: (2018). URL: https://em.geosci.xyz/content/physical_properties/dielectric_permittivity/index.html.

[6] Wanbiao Hu et al. "Electron-Pinned Defect-Dipoles for High-Performance Colossal Permittivity Materials". In: *Nature materials* 12 (June 2013). DOI: 10.1038/nmat3691.

[7] Tian Lan, Xiaoli Tang, and Brent Fultz. "Phonon anharmonicity of rutile TiO_2 studied by Raman spectrometry and molecular dynamics simulations". In: *Phys. Rev. B* 85 (9 Mar.

2012), p. 094305. DOI: 10.1103/PhysRevB.85.094305. URL: https://link.aps.org/doi/10.1103/PhysRevB.85.094305.

[8] P. S. Narayanan. "Raman spectrum of rutile". In: *Proceedings of the Indian Academy of Sciences - Section A* 37 (1953), pp. 411–414.

[9] Sergio P. S. Porto, Paul A. Fleury, and Theo C. Damen. "Raman Spectra of TiO_2, MgF_2, ZnF_2, FeF_2, and MnF_2". In: *Physical Review* 154 (1967), pp. 522–526.

[10] G. A. Samara and P. S. Peercy. "Pressure and Temperature Dependence of the Static Dielectric Constants and Raman Spectra of TiO_2 (Rutile)". In: *Phys. Rev. B* 7 (3 Feb. 1973), pp. 1131–1148. DOI: 10.1103/PhysRevB.7.1131. URL: https://link.aps.org/doi/10.1103/PhysRevB.7.1131.